Available online at www.sciencedirect.com
SCIENCE DIRECT®
Journal of Non-Crystalline Solids 351 (2005) 2166–2177
JOURNAL OF NON-CRYSTALLINE SOLIDS
www.elsevier.com/locate/jnoncrysol

Origin and enhancement of the second-order non-linear optical susceptibility induced in bismuth borate glasses by thermal poling

O. Deparis [a,*], F.P. Mezzapesa [a], C. Corbari [a], P.G. Kazansky [a], K. Sakaguchi [b]

[a] Optoelectronics Research Centre, University of Southampton, Southampton SO17 1BJ, United Kingdom
[b] Technical Research Laboratory, Nippon Sheet Glass Co., Ltd., Itami, Hyogo 664-8520, Japan

Received 30 July 2004; received in revised form 27 May 2005
Available online 6 July 2005

Abstract

The second-order non-linear optical susceptibility of thermally poled glasses, $\chi^{(2)}$, should be enhanced in proportion to the intrinsic third-order susceptibility $\chi^{(3)}$, for a given frozen-in electric field (i.e. $\chi^{(2)} = 3E_{dc}\chi^{(3)}$). In order to test this prediction, bismuth-borate (Bi_2O_3–ZnO–B_2O_3) glasses, for which $\chi^{(3)}$ increased with increasing Bi_2O_3 content, were thermally poled and the second-order non-linear coefficient was determined. Poling conditions and current dynamics turned out to be very different from those in silica. Poling temperatures had to be relatively close to glass transition temperatures and the glass–electrode contact had to be intimate in order to induce the non-linearity which was located in a near-surface layer at the anode side. A poling mechanism was proposed which relied on proton migration, took into account ion injection and glass ionization, and was able to explain most of the experimental results. The $\chi^{(2)}$ values increased with increasing $\chi^{(3)}$ as predicted but did not exceed 0.7 pm/V. By comparison with silica, it was inferred that the dielectric breakdown strength E_b was lower in bismuth borate and decreased with increasing Bi_2O_3 content. This latter result demonstrated the importance to select glass compositions on the basis of *both* $\chi^{(3)}$ and E_b for the purpose of enhancing $\chi^{(2)}$.

PACS: 42.70.−a; 72.20.−i; 72.80.−r; 77.22.−d

1. Introduction

Even-order non-linear optical interactions are forbidden in glass unless the (macroscopic) inversion symmetry of the amorphous network is broken intentionally. Breaking of the symmetry, which can be achieved by various poling techniques [1–5], provides the glass with second-order non-linear optical susceptibility $\chi^{(2)}$, which can be exploited in order to implement electro-optic and second-order non-linear effects in glass planar waveguides or optical fibres [6]. Among the available poling techniques, thermal poling has proven to be both straightforward and reliable [1]. The $\chi^{(2)}$ in thermally poled silica is of the order of 1 pm/V, possesses excellent long-term stability at room temperature and is determined mainly by the poling conditions [1]. In practice, the level of $\chi^{(2)}$ does not change significantly with the chemical composition of the glass although the latter has a dramatic influence on the stability of $\chi^{(2)}$ [7]. Thermal poling of glass involves creation and storage of an extremely high dc electric field ($\sim 10^8$ V/m) within the glass through charge migration at elevated temperature and subsequent freezing of the space charge. The second-order optical non-linearity, which is mainly located in a near-surface layer at the anode side, originates

* Corresponding author. Permanent address: Faculté Polytechnique de Mons, Electromagnetism and Telecommunications Department, 31 Boulevard Dolez, B-7000 Mons, Belgium. Tel.: +32 65 374194; fax: +32 65 374199.
E-mail addresses: olivier.deparis@fpms.ac.be, deparis@telecom.fpms.ac.be (O. Deparis).

0022-3093/$ - see front matter © 2005 Elsevier B.V. All rights reserved.
doi:10.1016/j.jnoncrysol.2005.06.004

from the rectification of the intrinsic third-order non-linear optical susceptibility $\chi^{(3)}$ by the frozen-in electrostatic field E_{dc} (i.e. $\chi^{(2)} = 3E_{dc}\chi^{(3)}$), although the orientation of dipoles by E_{dc} may contribute to the non-linearity as well [1,8]. The rectification model predicts that the maximum level of $\chi^{(2)}$ is set by the dielectric breakdown strength of the glass E_b, i.e. $E_{dc} < E_b$. In the case of silica, the predicted value of $\chi^{(2)}$ is about 0.5 pm/V ($E_b = 8 \times 10^8$ V/m, $\chi^{(3)} = 2 \times 10^{-22}$ m^2/V^2) and is in very good agreement with typical measured values. The rectification model also predicts that $\chi^{(2)}$ should increase proportionally to $\chi^{(3)}$, for a given value of E_{dc}. Enhancement of $\chi^{(2)}$ in proportion to $\chi^{(3)}$ is therefore expected in thermally poled glasses with higher $\chi^{(3)}$ than silica, provided that (1) the poling mechanism relying on charge migration is still valid for such glasses, (2) a frozen-in field strength as high as in silica can be achieved. High-index glasses, such as Bi_2O_3-based glasses, are potentially interesting for this purpose since they exhibit intrinsically high $\chi^{(3)}$ [9]. Based on this strategy, large second-order optical non-linearity has been reported in WO_3–TeO_2 glass [10].

In this article, we report on the physical origin and the enhancement of the second-order non-linear optical susceptibility induced in bismuth borate (Bi_2O_3–ZnO–B_2O_3) glasses by thermal poling. Glass samples, their chemical composition and relevant physical properties, the experimental set-up, the poling procedure and the non-linearity evaluation method are first presented. The results of poling and non-linear optical measurements are then reported and discussed in terms of poling mechanism, poling current dynamics and $\chi^{(2)}$ values. A poling mechanism is proposed which relies on proton migration and accounts for most of the experimental results. Measured values of $\chi^{(2)}$ are confronted to predictions of the rectification model.

2. Experimental conditions

2.1. Glass samples

Glass samples (BZH#) were fabricated by melting and quenching in the ternary Bi_2O_3–ZnO–B_2O_3 system and in the binary ZnO–B_2O_3 system (Table 1). Boron and zinc ions acted as network formers and modifiers, respectively. The bismuth oxide content was varied from 6.25 mol% to 25.0 mol% while keeping the ratio $r = [ZnO]_{mol\%}/([ZnO]_{mol\%} + [B_2O_3]_{mol\%})$ constant and equal to 0.5 (in the bismuth-free borate glass, this ratio was equal to 0.55). At low Bi_2O_3 content, bismuth ions acted as network modifiers whereas at high Bi_2O_3 content, bismuth ions acted both as network modifiers and network formers [11]. As the Bi_2O_3 content increased, the glass transition temperature (T_g) decreased while the glass density (ρ) and the refractive index (n) increased. The enhancement of $\chi^{(3)}$ (with respect to silica) could be estimated from Miller's rule [12], i.e. $\chi^{(3)} \div [\chi^{(1)}]^4$ with $\chi^{(1)} \div (n^2 - 1)$ (esu units). The enhancement factor $F = \left[(n^2 - 1)/(n_s^2 - 1)\right]^4$ increased from 4.7 to 33.3 as n increased from 1.62 to 1.91. Water was present in the glass matrix in the form of OH bonds (OH impurity level was in the range of a few hundreds of ppm and varied from batch to batch). Samples had thickness of 1.0 mm 0.5 mm or 0.2 mm and size of 20×30 mm^2. Optical transmission spectra exhibited a flat maximum between ~700 nm and ~2000 nm and an UV absorption edge which shifted toward longer wavelengths with increasing Bi_2O_3 content (Fig. 1). Assuming that the transmission loss in the flat region of the spectrum, T_0, was only due to Fresnel reflections at both air–sample interfaces (i.e. $T_0 = (1 - R^2)$ where R is the power reflection coefficient), the refractive index could be estimated by $n = [R^{1/2} + 1]/[1 - R^{1/2}]$. The values of n resulting from this estimation (Table 1) were slightly higher than those calculated from Sellmeier equation and coefficients reported for binary Bi_2O_3–B_2O_3 glasses with various Bi_2O_3 contents (Table 2). The higher values of n most likely resulted from the presence of zinc oxide in BZH samples. The refractive index dispersion ($\partial n/\partial\lambda$) was not measured but it was expected to increase with increasing Bi_2O_3 content, as it is the case in binary Bi_2O_3–B_2O_3 glasses [13]. Therefore, the coherence length of second-order non-linear optical interactions was expected to decrease with increasing Bi_2O_3 content. Based on Bi_2O_3–B_2O_3 glass dispersion data [13], the SHG coherence length was estimated to be four times lower in BZH2 samples (25.0 mol%

Table 1
Nominal compositions and physical properties of BZH samples

Sample	Bi_2O_3 (mol%)	ZnO (mol%)	B_2O_3 (mol%)	T_g (°C)	n	F	ρ (g/cm^3)	w_{OH} (wt%)
BZH6	–	55.0	45.0	550	1.62	4.7	~3.0	0.0624
BZH4	6.25	46.88	46.88	495	1.71	9.3	~4.0	0.0808
BZH7	12.5	43.75	43.75	470	1.79	16.0	~5.0	0.0531
BZH2	25.0	37.5	37.5	419	1.91	33.3	6.10	0.0463

T_g: glass transition temperature, n: refractive index, F: $\chi^{(3)}$ enhancement factor (with respect to silica), ρ: glass density, w_{OH}: weight percentage of hydroxyl (OH). Refractive index was estimated from Fresnel reflection loss measurements. The $\chi^{(3)}$ enhancement factor was calculated from Miller's rule: $F = [(n^2 - 1)/(n_s^2 - 1)]^4$, where n_s is the refractive index of silica ($n_s = 1.45$). The weight percentage of OH was calculated by: w_{OH} (%) $= 0.1 \times \alpha_{OH}/\varepsilon_{OH} \times M_{OH}/\rho$, where α_{OH} is the OH absorbance peak (measured at $\lambda \approx 2.9$ μm), ε_{OH} is the OH extinction coefficient (50 l/mol/cm) and M_{OH} is the OH molar weight. Values of w_{OH} are given for batches of 1.0 mm thick samples.

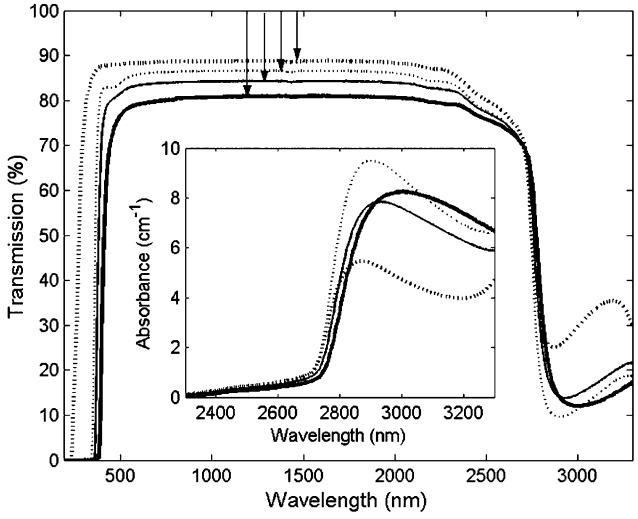

Fig. 1. Optical transmission spectra measured in 1.0-mm thick BZH6 (thick dotted line), BZH4 (thin dotted line), BZH7 (thin line) and BZH2 (thick line) samples. Vertical arrows indicate the transmission loss associated with Fresnel reflections at air/sample interfaces (T_0). Inset: absorbance spectra – the absorbance is calculated by $\alpha = [\log(1/T) - \log(1/T_0)]/d$, where T is the measured transmission loss and d is the sample thickness ($d = 1$ mm).

Bi_2O_3) than in silica (Table 2). The weight percentage of OH impurity was calculated from measurements of the absorbance peak around 2.9 μm (Fig. 1 – inset). The OH content ranged from 463 ppm in 1.0-mm thick BZH2 samples to 808 ppm in 1.0-mm thick BZH4 samples (Table 1) and varied from batch to batch (it was 1.5 times lower in 0.9-mm than in 1.0-mm thick BZH6 samples and two times lower in 0.2-mm than in 1.0-mm thick BZH2 samples).

2.2. Poling set-up and procedure

Samples were poled inside an oven (air atmosphere) using pressed-contact electrodes. The procedure consisted in heating slowly the sample up to a prescribed temperature (T_p), applying the voltage (V) for a certain time (t_p), cooling the sample slowly with the voltage still applied, and finally removing the voltage when the temperature became closer to room temperature (typically <50 °C). The sample with the electrodes was connected to a high-voltage power supply, a protection resistance (100 kΩ) and am-meter in serial configuration. The voltage was applied gradually from zero to the nominal value ($V = 4$ kV) within less than 1 min. The current (I) was recorded as a function of time from a few seconds before the voltage was applied to the end of the cooling. From measurement of the current at the time ($t = 0$) when the voltage had just reached nominal value, the electrical dc conductivity of the glass could be estimated according to $\sigma = I_{t=0}/V \times d/S$, where d is the sample thickness and S is the electrode area. Various combinations of poling temperature and time were tested. Different types of electrode were used, including silicon wafer, gold-on-silicon wafer, platinum foil and steel plate. Electrode size ranged from $S = 25$ mm^2 to 54 mm^2. Because of relatively low T_g values, BZH glasses underwent large thermal stresses during poling. In order to avoid breaking of the sample, heating and cooling had to be carried out slowly and the maximum poling temperature had to be scaled according to T_g.

2.3. Non-linearity evaluation method

In order to evaluate the second-order optical non-linearity, second-harmonic generation (SHG) was probed in the poled samples using p-polarized pump light from a mode-locked and Q-switched Nd–YAG laser ($\lambda_p = 1.064$ μm). The second-harmonic (SH) power generated from a non-linear layer of thickness w and probed at an incident angle θ_e can be expressed by [14]:

$$P_{2\omega}(\theta_e) = \frac{KP_\omega^2}{n_\omega^2 n_{2\omega}} \left| \int_0^w \chi_{zzz}^{(2)}(z) \exp\left(i \frac{\pi}{l_c \cos\theta_{2\omega}} z \right) dz \right|^2, \quad (1)$$

where z is the poling direction (perpendicular to the electrode surfaces), $\theta_{\omega(2\omega)} = \arcsin[\sin\theta_e/n_{\omega(2\omega)}]$ is the internal propagation angle of the pump (SH) wave, $l_c = \lambda_p/[4(n_{2\omega} - n_\omega)]$ is the SHG coherence length, P_ω is the pump power and $K = K(\theta_e, n_\omega, n_{2\omega})$ is a factor including the angular dependences of Fresnel transmission losses of pump and SH waves, the beam-shape correction factor and the projection factor of $\chi^{(2)}$ tensor. In poled glass $\chi^{(2)}$ tensor has $C_{\infty mm}$ symmetry: $\chi_{zzz}^{(2)} = 3\chi_{zxx}^{(2)}$, $\chi_{zxx}^{(2)} =$

Table 2
Second-order non-linear coefficient $\chi^{(2)}$ in poled BZH samples

Sample	d (mm)	T_p (°C)	t_p (min)	n_ω	$n_{2\omega}$	l_c (μm)	w (μm)	$\chi^{(2)}$ (pm/V)
BZH6	0.9	500	15	1.5500	1.5600	26.6	11.0†	0.15 (0.17)
BZH4	1.0	450	5	1.5600	1.5800	13.3	13.3	0.23 (0.29)
BZH	71.0	400	5	1.6580	1.6860	9.5	6.0†	0.38 (0.47)
BZH2	0.2	300	3	1.8106	1.8536	6.2	6.2	0.59 (0.68)

d: sample thickness, T_p: poling temperature, t_p: poling time, n_ω, $n_{2\omega}$: refractive index values at $\lambda = 1064$ nm and $\lambda/2 = 532$ nm, l_c: SHG coherence length, i.e. $l_c = \lambda/(4\Delta n)$ with $\Delta n = n_{2\omega} - n_\omega$, w: non-linear thickness. Values of n_ω and $n_{2\omega}$ were calculated using Sellmeier coefficients available for Bi_2O_3–B_2O_3 glasses [13]. Values of w were determined by etching and SHG measurements (†) or assumed to be equal to l_c. Values of $\chi^{(2)}$ were calculated from Eq. (2) using values of w, n_ω and $n_{2\omega}$ given in this Table (values of $\chi^{(2)}$ between parentheses were calculated using $n_\omega = n$ and $n_{2\omega} = n + \Delta n$, where the values of n are given in Table 1). Poling voltage: 4 kV.

$\chi^{(2)}_{zyy} = \chi^{(2)}_{yzy} = \chi^{(2)}_{xzx}$ (other elements being equal to zero). If the condition $w < l_c$ is satisfied (which is the case for BZH glasses, see Section 3), the exponential factor in Eq. (1) almost does not depend on z in the integration limits and is close to unity. In this case, Eq. (1) leads to

$$\chi^{(2)} \cong \frac{n_\omega \sqrt{n_{2\omega}}}{\sqrt{C}} \frac{\sqrt{P_{2\omega}}}{w}, \tag{2}$$

where $C = KP^2_\omega$ and $\chi^{(2)}$ is defined by

$$\chi^{(2)} = \frac{1}{w}\int_0^w \chi^{(2)}_{zzz}(z)\,\mathrm{d}z. \tag{3}$$

Unless we are interested in the spatial profile of the non-linearity, i.e. $\chi^{(2)}_{zzz}(z)$, Eq. (2) allows us to determine is the spatially averaged non-linearity, i.e. $\chi^{(2)}$, directly from $P_{2\omega}$, provided that C, w, n_ω, and $n_{2\omega}$ are known. We evaluated $\chi^{(2)}$ by first recording $P_{2\omega}$ as a function of θ_e, i.e. the so-called Maker fringe (MF) curve [15]. The factor C was calculated from calibration measurements using a quartz plate ($\chi^{(2)}_{xxx} = 0.6$ pm/V). The non-linear thickness was determined by etching the poled area and measuring the decay of $\sqrt{P_{2\omega}}$ as a function of the etched depth (or it was simply assumed to be equal to the SHG coherence length). The refractive index at pump and SH wavelengths were calculated using Sellmeier coefficients and equation reported for binary Bi_2O_3–B_2O_3 glasses with various Bi_2O_3 content [13]. In principle, knowing C, w, n_ω, and $n_{2\omega}$, we could calculate $\chi^{(2)}$ from $P_{2\omega}$ measured *at any angle*. In order to increase the accuracy, we calculated $\chi^{(2)}$ by fitting the recorded MF curve with $\chi^{(2)}$ as the only parameter. Non-linear thickness measurements are time consuming and, for this reason, we did not performed them systematically on all the samples. Instead, we used a normalized quantity, η_{SHG}, defined by

$$\eta_{SHG} = \frac{P_{2\omega}}{P_{2\omega,ref}} = \frac{n^2_{\omega,ref} n_{2\omega,ref}}{n^2_\omega n_{2\omega}} \frac{C}{C_{ref}} \left(\frac{\chi^{(2)} w}{\chi^{(2)}_{ref} w_{ref}}\right)^2, \tag{4}$$

where $P_{2\omega}$ and $P_{2\omega,ref}$ were measured at a fixed incident angle ($\theta_e = 60 \pm 1°$) in the poled sample under test and in a reference sample (0.5-mm thick Herasil® silica plate, poled at 280 °C and 4 kV for 30 min), respectively. Measurements were performed at different locations in the poled area in order to check the uniformity of SHG. On the basis of η_{SHG}, a comparison could be made between poled samples in terms of the squared product of non-linear thickness and spatially averaged non-linear coefficient.

3. Results

Poling had to be carried out at temperatures relatively close to T_g in order to induce second-order optical non-linearity in BZH samples. On overall SHG of the same order of magnitude as in silica ($\eta_{SHG} = 1$) was obtained by poling at temperatures ranging from $0.75 \times T_{g,K}$ to $0.95 \times T_{g,K}$, the optimal temperature depending on Bi_2O_3 content and, surprisingly, on sample thickness (Fig. 2). For BZH6 glass (bismuth-free), highest values of η_{SHG} were obtained in 0.9-mm thick samples poled at 500 °C ($0.94 \times T_{g,K}$). For BZH4 glass (6.25 mol% Bi_2O_3), highest values of η_{SHG} were obtained in 1.0-mm thick samples poled at 420 °C ($0.90 \times T_{g,K}$). For BZH7 glass (12.5 mol% Bi_2O_3), high values of η_{SHG} were obtained both in 1.0-mm and 0.2-mm thick samples poled at 400 °C ($0.91 \times T_{g,K}$) and 350 °C ($0.84 \times T_{g,K}$), respectively. For BZH2 glass (25.0 mol% Bi_2O_3), high values of η_{SHG} were obtained only in 0.2-mm thick samples poled around 280 °C ($0.80 \times T_{g,K}$).

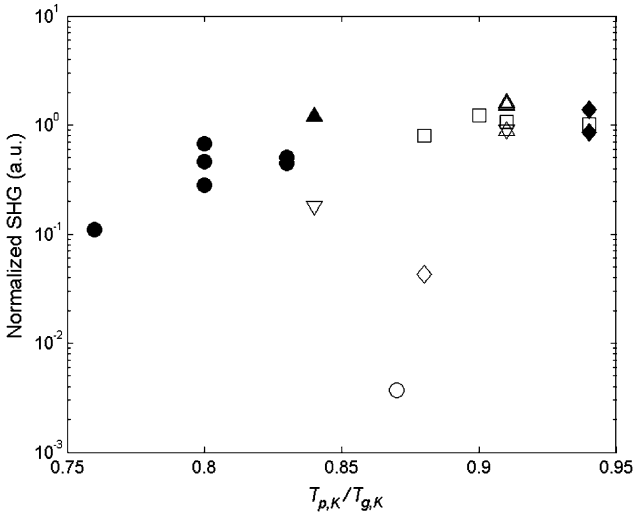

Fig. 2. Normalized SHG (η_{SHG}) as a function of the ratio between poling and glass transition absolute temperatures ($T_{p,K}/T_{g,K}$) for BZH6 (◇, ◆), BZH4 (□), BZH7 (△, ▽, ▲) and BZH2 (○, ●) samples. Samples were poled at 4 kV for different times. Highest values of η_{SHG} (with respect to poling time) are displayed for each glass. Samples thickness: 1.0 mm (◇, □, △, ○), 0.9 mm (◆), 0.5 mm (▽), 0.2 mm (▲, ●).

At a given poling temperature, η_{SHG} depended on the poling time (Fig. 3). In 0.9-mm thick BZH6 samples, poling time of at least 15 min was required to achieve significant SHG at 500 °C. In 1.0-mm thick BZH4 samples, longer poling time led to higher SHG at 420 °C but the trend was opposite at 450 °C. In 1.0-mm (0.2-mm) thick BZH7 samples, SHG increases with poling time at 400 °C (350 °C), reached a maximum after ~5 min and then decreased for longer poling time. Note that similar dynamics was reported in thermally poled silica [16]. In 0.2-mm thick BZH2 samples, a short poling time (~5 min) was sufficient to achieve maximum SHG at 280 °C while a longer time (~30 min) was needed at 250 °C. Unexpectedly, a strong dependence of η_{SHG} on sample thickness was observed in BZH7 samples (Fig. 3 – inset). After poling at 350 °C for 5 min, η_{SHG} in 0.2-mm thick samples was two orders of magnitude higher than in 1.0-mm thick samples.

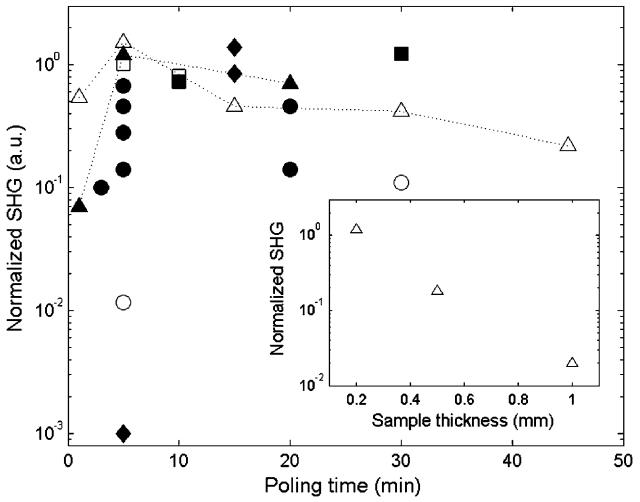

Fig. 3. Normalized SHG (η_{SHG}) as a function of poling time for BZH6 (◆), BZH4 (□, ■), BZH7 (△, ▲) and BZH2 (○, ●) samples. Samples were poled at 4 kV at different temperatures: 500 °C (◆), 450 °C (□), 420 °C (■), 400 °C (△), 350 °C (▲), 280 °C (●), 250 °C (○). Samples thickness: 1.0 mm (◇, □, ■, △), 0.9 mm (◆), 0.2 mm (▲, ○, ●). Dotted lines connect data. Inset: normalized SHG as a function of the sample thickness in BZH7 samples poled at 4 kV and 350 °C for 5 min using gold-on-silicon wafer electrodes.

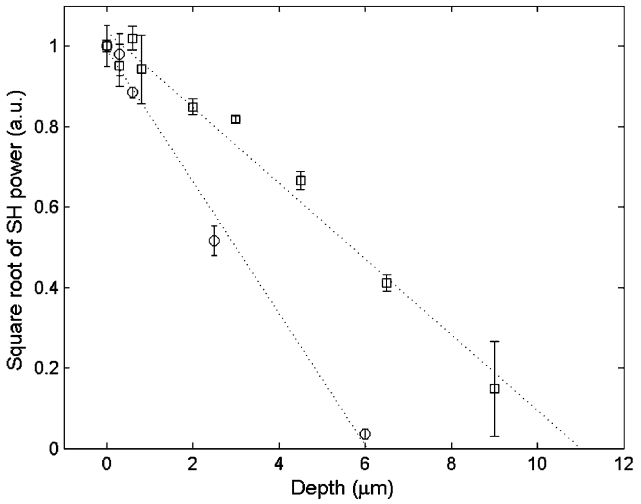

Fig. 4. Determination of the non-linear thickness in BZH6 (□) and BZH7 (○) samples by successive etching and SHG measurements – the square root of SH power is plotted as a function of the etched depth. Error bars indicate standard deviations of the measured quantity across the poled area. Dotted lines are best linear fits to data. The non-linear thickness is given by the intercept of the best linear fit with the x-axis. Poling conditions: 4 kV, 500 °C, 15 min (□); 4 kV, 400 °C, 5 min (○). Electrodes: gold-on-silicon. Samples thickness: 0.9 mm (□), 1.0-mm (○).

Etching of poled samples in diluted nitric acid revealed that the non-linearity was located in a thin layer underneath the sample surface which was in contact with the anode during poling. Assuming a step profile for the non-linearity ($\chi^{(2)}_{zzz}(z) = \chi^{(2)},\ 0 \leqslant z < w;\ \chi^{(2)}_{zzz}(z) = 0, w \leqslant z \leqslant d$), the square root of SH power is expected to decrease linearly with increasing etched depth, the depth at which this quantity drops to zero being equal to the thickness of the non-linear layer (cf. Eq. (2)). Such a linear dependence was found with good approximation in 0.9-mm thick BZH6 and 1.0-mm thick BZH7 samples poled at 500 °C for 15 min and at 400 °C for 5 min, respectively (Fig. 4). For these poling conditions, non-linear thickness values of 11.0 ± 0.5 μm and 6.0 ± 0.5 μm were determined, respectively. In 1.0-mm thick BZH7 sample poled at 400 °C for 30 min, a non-linear thickness values of 6.56 ± 0.84 μm was determined using non-destructive stack Maker fringe technique [17]. This result shows that, although the non-linear thickness was higher for longer poling time, the steady-state was almost reached after ~5 min.

The shape of Maker fringe curves showed that, for all BZH samples, the non-linearity was located mainly in a layer whose thickness was lower than SHG coherence length, in agreement with etching measurements (Fig. 5). Provided that $w < l_c$, the shape of MF curves does not change much as w is varied: $P_{2\omega}$ increases as the path length in the non-linear layer increases (i.e. as θ_e increases) and then decreases at large angles due to Fresnel losses [14]. Although the non-linear thickness was not determined in BZH4 and BZH2 samples (e.g. by etching), the shape of MF curves indicated that $w < l_c = 13.3$ μm and $w < l_c = 6.2$ μm, respectively. In some samples (e.g. BZH7 sample poled at 400 °C for 30 min), a slight over-modulation with a period corresponding to the sample thickness was observed in the MF curve. This feature indicated that a weak non-linearity was present either in the bulk or in a thin layer at the cathode side [18].

The electrical dc conductivity (σ) of BZH glasses was measured at various temperatures (Figs. 6 and 7) and the associated activation energy E_σ was determined (Fig. 7 – inset). These measurements revealed that: (1) σ changed dramatically with glass composition (and from batch to batch in the case of BZH6 samples); (2) correlations existed between σ and T_g and between σ and the Bi_2O_3 content: the lower (higher) the glass transition temperature (Bi_2O_3 content), the higher the conductivity at a given temperature; (3) E_σ depended on glass composition. The activation energy E_σ was equal to ~1.5 eV in BZH7 glass and BZH2 glass, ~2.5 eV in BZH4 glass and ~2.2 eV in BZH6 glass. These values of E_σ are higher than the value of ~1 eV reported for thermal dissociation of Na^+ in silica [19], which is responsible for the ionic conductivity of flame-fused silica. Because charge transport mechanisms in BZH glasses involve both electronic and ionic conductivity (see Section 4), the activation energy E_σ can not be simply associated with the motion of a single charge carrier, like in silica.

Different evolutions of the poling current with time were observed depending on glass composition, poling

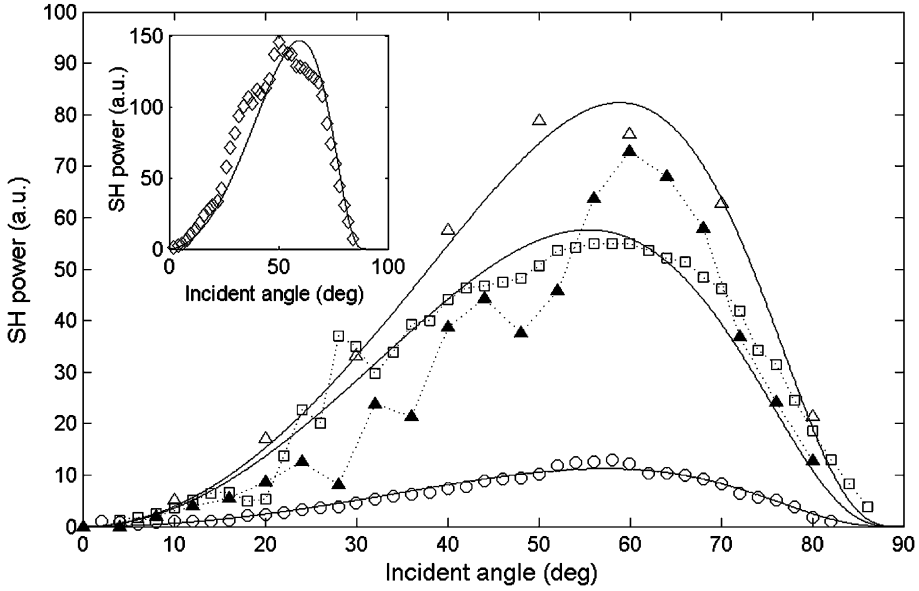

Fig. 5. Maker fringe curves measured on BZH6 (◇, inset), BZH4 (□), BZH7 (△, ▲) and BZH2 (○) poled samples. Poling voltage: 4 kV. Poling temperature: 500 °C (◇), 450 °C (□), 400 °C (△, ▲), 300 °C (○). Poling time: 15 min (◇), 5 min (□, △), 30 min (▲), 3 min (○). Sample thickness: 0.9 mm (◇), 1.0 mm (□, △, ▲), 0.2 mm (○). Dotted lines connect data. Lines are best fits to Maker fringe theoretical curves using non-linear thickness of 11.0 μm (◇), 13.3 μm (□), 6.0 μm (△) and 6.2 μm (○).

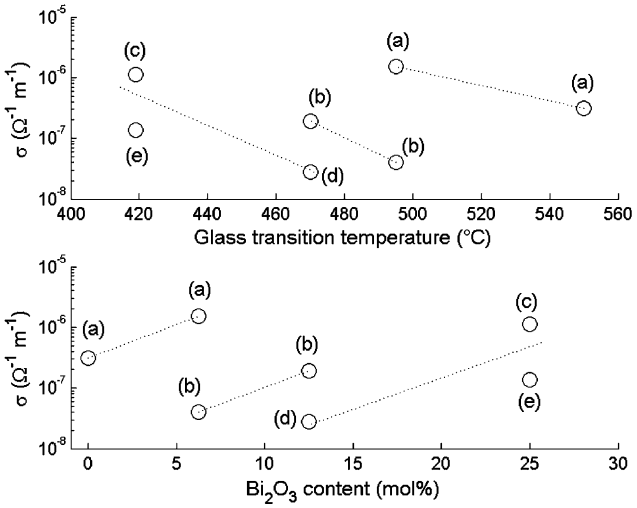

Fig. 6. Electrical dc conductivity (σ) of BZH glasses at various temperatures as a function of glass transition temperature and bismuth oxide content. The labels next to data indicate the temperature at which the conductivity was measured: 450 °C (a), 400 °C (b), 370 °C (c), 350 °C (d) and 330 °C (e). Sample thickness: 1.0 mm (a, b), 0.2 mm (c–e). Dotted lines are only guides for the eyes.

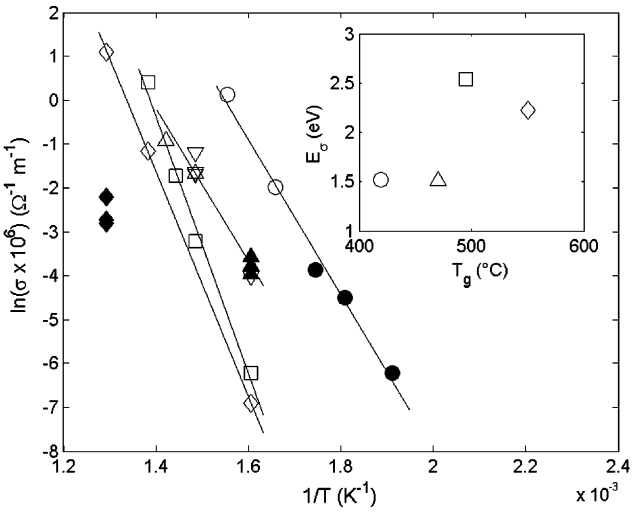

Fig. 7. Electrical dc conductivity (σ) as a function of reciprocal absolute temperature in BZH6 (◇, ◆), BZH4 (□), BZH7 (△, ∇, ▲) and BZH2 (○, ●) samples. Sample thickness: 1.0 mm (◇, □, ○, △), 0.9 mm (◆), 0.5 mm (∇), 0.2 mm (▲, ●). Lines are best linear fits to Arrehnius law: $\sigma = \sigma_0 \times \exp[-E_\sigma/k_B\,T]$, where is σ_0 the pre-exponential factor, E_σ is the activation energy, k_B is the Boltzmann constant and T is the absolute temperature. Inset: activation energy as a function of glass transition temperature.

temperature and sample thickness (Fig. 8). The level of poling current ranged from tens to hundreds of microamperes for typical poling conditions. In BZH6 samples from a second batch (0.9-mm thick), the current dynamics were significantly different than in BZH6 samples from a first batch (1.0-mm thick). In BZH4 and BZH7 samples, the current evolved slowly with time (either decreased or increased depending on poling temperature and sample thickness). In BZH2 samples, the current increased rapidly with time with a tendency to saturation. For identical poling conditions, the type of electrode used as anode had a strong influence on the current dynamics (Fig. 9) and on the SHG (Table 3). In 1.0-mm thick BZH6 samples poled at 500 °C, the current dynamics changed dramatically when the

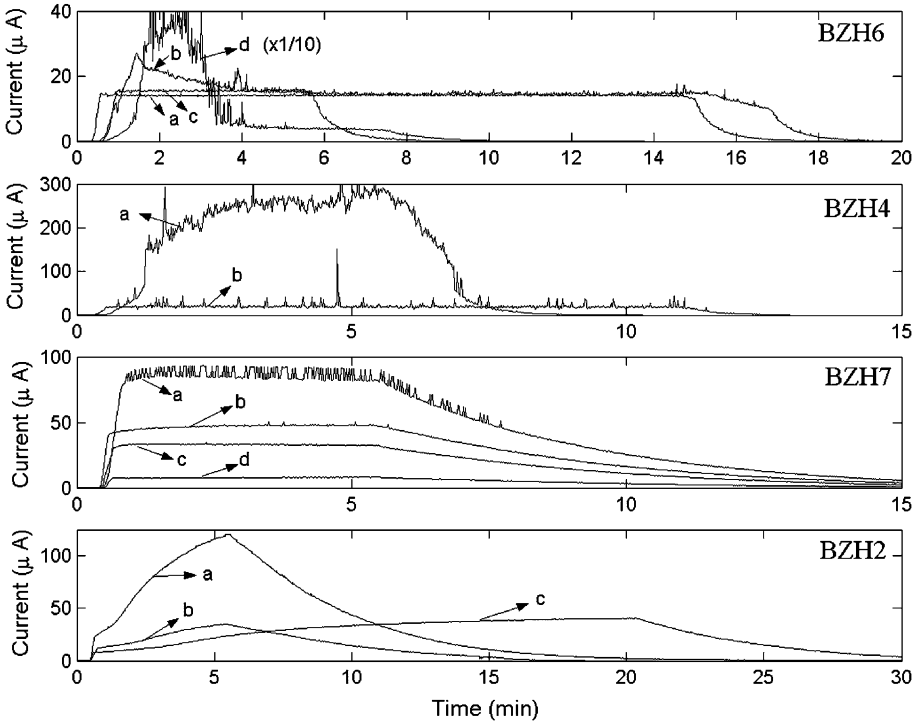

Fig. 8. Poling current dynamics in (from top to bottom charts) BZH6, BZH4, BZH7 and BZH2 samples. Poling voltage: 4 kV. Poling temperature – BZH6: 500 °C (a–d); BZH4: 450 °C (a), 420 °C (b); BZH7: 400 °C (a, b), 350 °C (c, d); BZH2: 300 °C (a), 280 °C (b, c). Poling time – BZH6: 15 min (a, b), 5 min (c, d); BZH4: 5 min (a), 10 min (b); BZH7: 5 min (a–d); BZH2: 5 min (a, b), 20 min (c). Sample thickness – BZH6: 0.9 mm (a–c), 1.0 mm (d); BZH4: 1.0 mm (a, b); BZH7: 1.0 mm (b), 0.5 mm (a, d), 0.2 mm (c); BZH2: 0.2 mm (a–c). Electrode – BZH6: 6×9 mm^2 gold-on-silicon wafer (a–c), 4×4 mm^2 polished silicon wafer (d); BZH4: 5×5 mm^2 polished silicon wafer (a, b); BZH7: 6×9 mm^2 gold-on-silicon wafer (a–d); BZH2: 6×9 mm^2 polished silicon wafer (a, c), 6×9 mm^2 gold-on-silicon wafer (b).

non-polished side instead of the polished side of a silicon wafer was used as electrode. Actually, field-assisted metal-to-glass sealing or anodic bonding [20] occurred in the latter case whereas it did not happen in the former case. In 1.0-mm thick BZH7 samples poled at 400 °C, evolutions of the current with time were dependent on the type of electrode. Moreover, the flatter the electrode surface, the higher and the more uniform the SHG in the poled area (Table 3). From these results, it appeared that the contact between the electrode and the glass surface was responsible for changes in current dynamics and variations in SHG. Intimate contact turned out to be essential for achieving high and uniform SHG.

The sample thickness had a strong influence on the poling current dynamics as well. Before reporting on this effect, it is worth to note that the poling temperature (or voltage) had to be reduced for thin samples in order to avoid the flow of high currents (>1 mA) which eventually caused dielectric breakdown ($I = V \times S/d \times \sigma(T)$). At a poling temperature of 400 °C (350 °C), the current increased slowly with time in 1.0-mm (0.5-mm) thick BZH7 samples whereas it decreased slowly with time in 0.5-mm (0.2-mm) thick BZH7 samples (Fig. 8). At 400 °C, the change in current dynamics was even more dramatic between 1.0-mm and 0.2-mm thick samples, despite the voltage had to be reduced by a factor of two in the latter case in order to avoid dielectric breakdown (Fig. 10). Faster decrease of the current was ob-

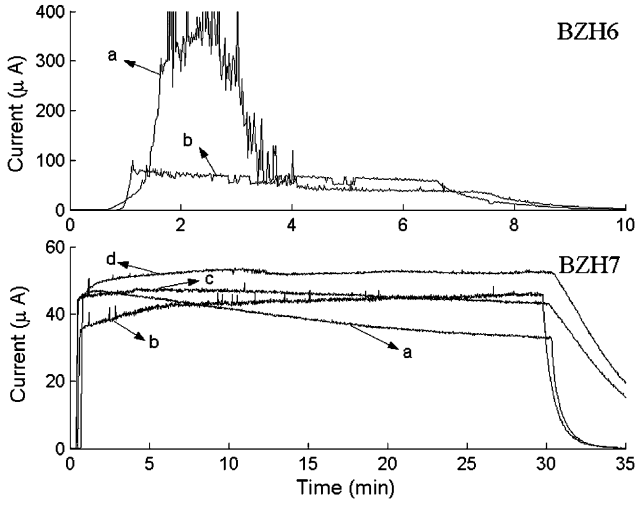

Fig. 9. Poling current dynamics in BZH6 (top chart) and BZH7 (bottom chart) samples, poled with different type of electrodes. Poling voltage: 4 kV. Poling temperature and time were kept constant – BZH6: 500 °C, 5 min; BZH7: 400 °C, 30 min. Electrode type – BZH6: polished silicon wafer (a), non-polished silicon wafer (b); BZH7: polished silicon wafer (a), non-polished silicon wafer (b), gold-on-silicon wafer (c), steel plate (d). Electrode size – BZH6: 5×5 mm^2 (a), 8×6 mm^2 (b); BZH7: 69 mm^2 (a–d). Sample thickness: 1.0 mm.

Table 3
Normalized SHG in BZH samples poled with different types of electrode

Glass	Electrode type	η_{SHG}
BZH6	Pt	$(0.7–4.0)\times10^{-3}$
	Si	$\sim4.3\times10^{-2}$
BZH4	Pt	$(0.1–1.3)\times10^{-2}$
	Si	~1.22
	s	$\sim10^{-3}$
BZH7	Si	0.05–0.11
	Au	0.33–0.54
	Si†	$(0.5–1.6)\times10^{-3}$
	s	0.11–0.16

Platinum foil (Pt), polished silicon wafer (Si), non-polished silicon wafer (Si†), gold-on-silicon wafer (Au), steel plate (s).
Electrode roughness increased in the following order: polished silicon wafer (<10 nm), gold-on-silicon wafer (<50 nm), steel plate (<100 nm), non-polished silicon wafer (~1000 nm), platinum foil. Poling voltage: 4 kV. Poling temperature and time were kept constant for poling with different electrodes: 450 °C, 5 min (BZH6); 420 °C, 30 min (BZH4); 400 °C, 30 min (BZH7). Sample thickness: 1.0 mm.

served in 0.2-mm thick sample ($V = 2.0$ kV) than in 1.0-mm thick sample ($V = 4.0$ kV).

We also checked that the second-order non-linearity could be erased by thermal annealing. In a 1-mm thick poled BZH7 sample (400 °C, 4 kV, 5 min) in which η_{SHG} was equal to 0.89, SHG could not be detected anymore after thermal annealing at 350 °C for 15 min. In contrast with the reversible character of the induced second-order optical non-linearity, irreversible changes in the chemical properties of Bi-containing BZH glasses were induced by thermal poling. After poling of BZH7 and BZH2 samples, a precipitate was formed on the cathode side (Fig. 11). The precipitate was confined within the electrode edges and was darker and denser in BZH2 than in BZH7 samples. The amount of precipitate increased with poling time. Etching revealed that the precipitate extended to a depth of at least 1 μm under the cathodic surface. Chemical element analysis of the precipitate was performed by EDX spectroscopy using a scanning area of 20×30 μm^2, which typically covered a single hill-like feature such as those shown in SEM images of Fig. 11 (inset). The weight percentage of ZnO (nominal value: 28.64 wt%) was practically unchanged inside and outside the feature (29.36 wt% and 27.07 wt%, respectively). On the other hand, the weight percentage of Bi_2O_3 (nominal value: 46.85 wt%), although it was practically unchanged outside the feature (47.65 wt%), was significantly decreased inside the feature (41.88 wt%).

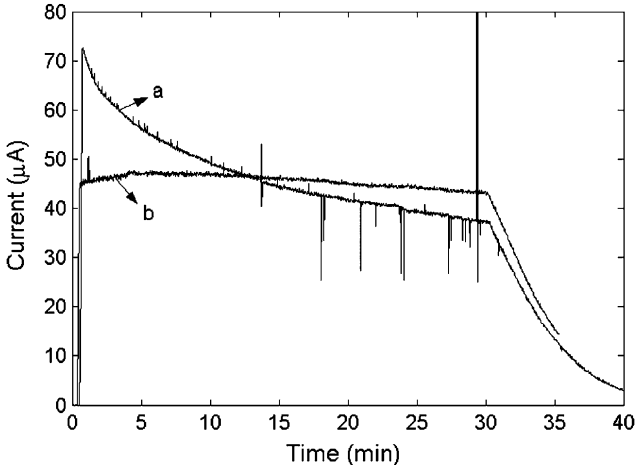

Fig. 10. Poling current dynamics in 0.2-mm (a) and 1.0-mm (b) thick BZH7 samples. Poling voltage: 2 kV (a), 4 kV (b). Poling temperature: 400 °C. Poling time: 30 min. Electrodes: 6×9 mm^2 gold-on-silicon wafer.

The values of $\chi^{(2)}$ were determined using Eq. (2) for typical poling conditions (Table 2). The $\chi^{(2)}$ values in thermally poled BZH glasses depended on Bi_2O_3 content, and therefore on $\chi^{(3)}$: they increased with increasing values of $\chi^{(3)}$ (Fig. 12). On overall, $\chi^{(2)}$ was of the same order of magnitude as in thermally poled silica. Concerning this calculation, we would like to point out that (1) only the lower limit of $\chi^{(2)}$ was obtained when non-linear thickness values equal to the coherence length were used instead of measured values, (2) slightly underestimated $\chi^{(2)}$ was obtained using calculated refractive index values because they were slightly lower than actual refractive index values of BZH glasses (cf. Section 2.1).

4. Discussion

4.1. Poling mechanism

The poling conditions which were required to induce second-order optical non-linearity in bismuth borate (Bi_2O_3–ZnO–B_2O_3) and borate (ZnO–B_2O_3) BZH glasses were significantly different from those used for silica. First of all, in silica, efficient poling is achieved at temperatures ranging from 250 °C to 350 °C far below glass transition temperature (~1100 °C) whereas, in BZH glasses, efficient poling is achieved only at temperatures relatively close to T_g. Secondly, intimate glass–electrode contact must be achieved in order to pole BZH glasses efficiently, whereas it has not been reported to be essential for poling of silica. Differences are noticed in poling current dynamics as well. In silica, the poling current is of the order of 1 μA for typical poling conditions (280 °C, 4 kV) and it decays rapidly with time (~1 min) as a result of the formation of a cation-depleted near-surface layer at the anode side which acquires a much higher resistivity than the bulk [21]. In BZH glasses, the poling current is much higher (10–100 μA) and exhibits very different dynamics depending on Bi_2O_3 content. In silica, varying the sample thickness (d) changes the time constant associated with the decay

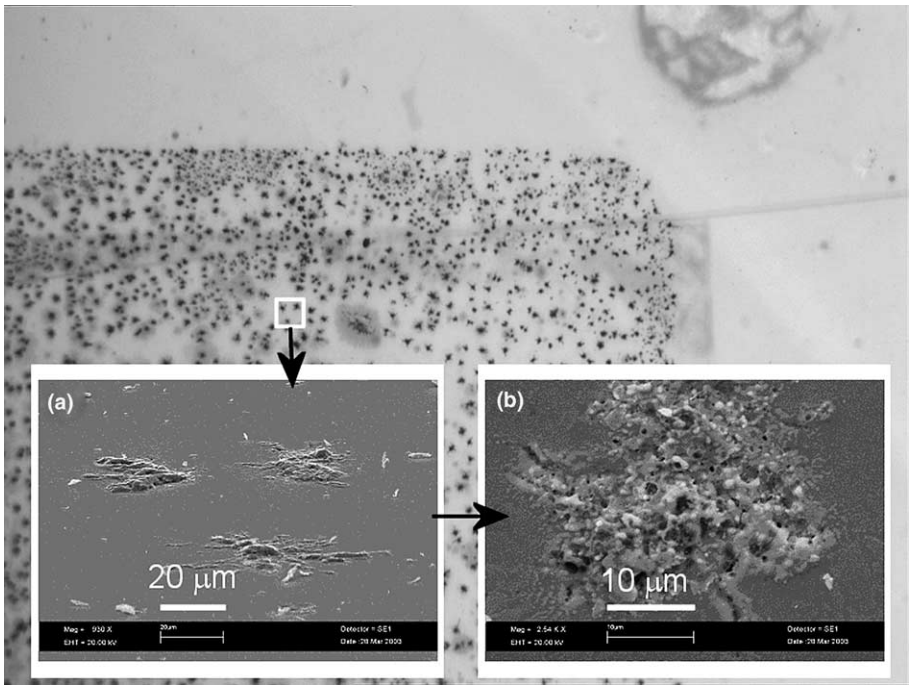

Fig. 11. Optical microscope image (magnification ×2) of the cathodic surface of poled BZH7 sample. Poling conditions: 4 kV, 400 °C, 30 min, gold-on-silicon electrodes. Dark spots appeared on the cathodic surface (within electrode area) as a result of poling. Inset: scanning electron microscope (SEM) images of three typical spots (a) and of a single spot (b).

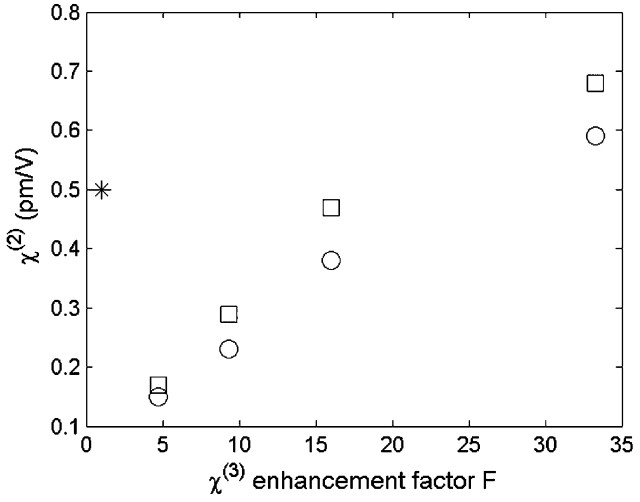

Fig. 12. Values of $\chi^{(2)}$ in thermally poled BZH glasses as a function of $\chi^{(3)}$ enhancement factor F (with respect to silica). The graph was plotted using values of F in Table 1 and the values of $\chi^{(2)}$ (circles) in Table 2 (squares: values of $\chi^{(2)}$ between parentheses in Table 2). The typical level of $\chi^{(2)}$ in thermally poled silica ($F = 1$) is indicated by a star.

of the poling current ($\tau \div d$) but does not change significantly the formation dynamics and the amount of $\chi^{(2)}$ [16]. In BZH glasses, varying the sample thickness results in dramatic changes in the formation dynamics and the amount of $\chi^{(2)}$. In spite of these differences, the non-linearity is confined within a near-surface layer at the anode side, like in silica.

The conductivity of BZH glasses is different from that of silica. In flame-fused silica, sodium ions (Na^+) are the most mobile charge carriers at typical poling temperatures and are responsible for the initial build up of the space charge field underneath the anodic surface [22]. Once the space charge field has reached very high values (close to dielectric breakdown), injection of ionized species from the atmosphere (H^+, H_3O^+) [23] and ejection of negative charges (electrons or oxygen ions) [8,24] can take place at the anode, modifying the distribution of the space charge across the depth. The nature of the conductivity in bismuthate glasses is not clearly established yet. Ionic conduction has been suggested in the case of bismuth silicate and bismuth germanate, where it is believed that oxygen ions are the charge carriers and percolation in the BiO_{5-6} sub-network is the charge transport mechanism [25]. In thermal poling experiment, migration of oxygen ions would result in an anion-depleted layer underneath the cathodic surface where second-order non-linearity would be located. Since SHG arose from anode side and not from cathode side of poled BZH glasses, we concluded that the above mentioned conduction mechanism did not apply here. Electronic conduction has been reported in bismuth borate [26], which basically involves electron hopping between bismuth ions of different valence states (Bi^{3+} and Bi^{5+}). This conduction mechanism could explain the dramatic increase of conductivity with increasing Bi_2O_3 content, which was observed in BZH glasses. However, the increase of

Bi_2O_3 content is accompanied by a decrease of T_g which is likely to affect the conductivity at a given temperature. At temperatures relatively close to T_g, we believe that proton conduction takes place in BZH glasses. Proton conduction, which has been evidenced in hydrous $BaSi_2O_5$ glass [27], is associated here with the presence of hydroxyl (OH) in all BZH samples.

Assuming that protons and electrons are the mobile charge carriers, we propose the following model for the poling mechanism in BZH glasses which accounts for most of the experimental results. Let us first assume a perfect contact between the electrode (anode) and the sample surface (this is practically the case with polished silicon wafer or gold-on-silicon wafer). Applying high voltage to the sample at elevated temperatures results in the dissociation of OH bonds and the release of protons (H^+). The mobility of H^+ carrier is likely to be enhanced near T_g. Under the action of the applied electric field, protons migrate toward the cathode, leaving negatively charged dangling bonds ($B–O^-$) behind them. As a result a space charge field builds up under the anode, which peaks at the surface, decreases linearly with depth in the proton-depleted layer and is constant across the rest of the bulk [28]. On the other hand, dangling bonds being more flexible near T_g, partial orientation of the electrical dipoles associated with these bonds may occur in the direction opposite to the applied electric field. Freezing of the space charge field and/or dipole orientation results in the creation of $\chi^{(2)}$ through the rectification of $\chi^{(3)}$ by the internal dc field and/or through individual contributions of dipole hyperpolarizability. This simple model is already able to explain two important experimental results: (1) the location of the non-linearity in a near-surface layer at the anode side, (2) the need of poling temperature relatively close to T_g. Anodic bonding, which was observed after poling of borate BZH6 glass at 500 °C using polished silicon wafer electrode, can be explained as well. It resulted from electric-field assisted bonding between $\equiv Si^+$ (wafer) and $B–O^-$ (sample) at the glass–electrode interface. For a more accurate description of the poling mechanism, one must take into account the possibility of ionization and ion injection driven by high electric field. Ionization can take place if the electric field strength in the glass exceeds its dielectric breakdown strength, giving rise to, e.g. emission of electrons at the anode. Injection of ions can take place because of the high field which builds up under the anode as a result of the formation of the proton-depleted layer. If the glass–electrode contact is not perfect (this is the case with non-polished silicon wafer or steel plate), ionized species from the atmosphere which are attracted by this high field penetrate into the sample and diffuse in the depth. The injected ions can recombine with fixed negative charges left by the migration of internal ions or, in other words, injected ions substituted to internal ions in analogy with an ion-exchange process. Such a process is known to take place during thermal poling of silica but it does not have a crucial impact on the non-linearity because the substitution ions (H^+ or H_3O^+) have a much lower mobility than the internal ions (Na^+) [23]. In the case of BZH glasses, on the other hand, substitution ions and internal ions are either the same (H^+) or similar (H_3O^+ and H^+) and therefore the ion-exchange process is believed to be much more efficient. The competition between release of internal H^+ (formation of $B–O^-$) and injection of H^+ or H_3O^+ (neutralization of $B–O^-$) has a net effect which depends on injection and poling conditions. The above considerations explain why the non-linearity is so critically dependent on the glass–electrode contact in the case of BZH glasses. In Bi-containing BZH glasses, we believe that electron hopping between Bi ions of different valence sates does not contribute to the formation of the non-linearity although it does contribute to the poling current. Unlike ions, electrons can not be blocked at the electrodes and therefore can not create a depletion (or accumulation) near-surface space charge layer. They can be involved, however, in reduction–oxidation chemical reactions at the glass–electrode interfaces (the precipitate which was observed at the cathode side in BZH7 and BZH2 samples is attributed to reduction of bismuth).

4.2. Poling current dynamics

The dynamics of the poling current can be qualitatively explained by considering the equivalent electrical dc circuit of the sample. As far as the different charge transport processes can be considered as independent from each other, the current in the external circuit is the summation of the currents associated with each process (parallel circuit):

$$I = I_{mig} + I_{inj} + I_{ion} + I_{hop}, \tag{5}$$

where I_{mig}, I_{inj}, I_{ion} and I_{hop} are the currents associated with migration of internally released protons, injection of foreign cations, ionization of the glass and electron hopping between multi-valent bismuth ions, respectively. The second term can be regarded as a consequence of the proton depletion process. The same comment holds for the third term, although it could appear in the absence of ion depletion (ionization would take place in the whole bulk in this case). The fourth term is relevant for Bi-containing glasses only.

The dynamics of I_{mig} is known from early studies on ion migration in crystals [28] and glasses [29–31] in the case of blocking electrodes. In this case, the current decays with a time constant which is given by [28]:

$$\tau = d/\mu\sqrt{\varepsilon/(2qNV)}, \tag{6}$$

where ε, q, μ and N are the dielectric constant, the elementary electric charge, the carrier mobility and

concentration, respectively. The dynamics of I_{inj} depends on the evolution of the electric field strength E_{dc} with time and the glass–electrode contact ($I_{inj} \neq 0$ if the contact is not perfect and E_{dc} at the anode is high enough to attract ions from the atmosphere). The injection of ions modifies the distribution of E_{dc} in the depth due to charge neutralization in the depletion layer, which in turns changes the injection conditions. The dynamics of I_{ion} depends on the evolution of E_{dc} with time and the dielectric breakdown strength E_b ($I_{ion} \neq 0$ only if $E_{dc} \geqslant E_b$). Ionization of the glass modifies the distribution of E_{dc} through charge ejection from the depletion layer. The dynamics of I_{hop} is expected to be non-stationary in the presence of mixed ionic-electronic conductivity (e.g. [32]), but the complexity of the problem makes current dynamics difficult to predict.

In bismuth-free BZH6 glass poled at 500 °C, the initial level of current was higher in samples from the first batch which contained higher concentration of OH impurity. This result supports our hypothesis of migration of internally released protons. In these samples, decay of the current was observed and was much faster when intimate glass–electrode contact was realized. This result supports our hypothesis of ion injection which slows down the formation of the depletion layer. In samples from the second batch, decay of the current was not observed systematically. In all samples, the current evolved towards a steady level. Such a constant current is tentatively assigned to ionization of the glass. Ion injection and ionization are believed to make difficult the identification of proton migration from poling current dynamics. In bismuth-containing BZH glasses, the electronic current makes poling current dynamics even more difficult to interpret. In BZH4 samples, one can only infer that the contribution of proton migration is much weaker than the other contributions. In BZH7 samples, the changes of current dynamics with sample thickness and poling temperature tend to support our model. Indeed, by changing adequately these parameters, opposite dynamics were observed, namely the current decreased (increased) with time as the poling temperature was increased (decreased) and/or the thickness was decreased (increased). Assuming that the decay of the current is due to proton migration, this result is consistent with the decrease of the related decay time constant with increasing temperature (i.e. increasing mobility) and decreasing sample thickness (cf. Eq. (6)). In BZH2 samples, the non-linearity was formed in a short period of time (typically 5 min) during which the current increased rapidly and then saturated. The electronic current is expected to increase dramatically with increasing Bi_2O_3 content and is likely to be the dominant conduction process in BZH2 glass, hiding the contribution of proton migration in the poling current dynamics. Increase and saturation of the poling current appear to be peculiar features of BZH glasses with high Bi_2O_3 content. Further experiments are needed to understand more deeply the poling mechanism and, by this way, to increase the values of $\chi^{(2)}$ in BZH glasses. For example, according to our model, it is worth to apply the voltage in small amplitudes steps in order to let the depletion region form progressively, in analogy with the procedure which is used for poling soda lime glasses [33].

4.3. Origin of precipitate on the cathodic surface

SEM images showed that the precipitate consisted of spots coming out the glass surface like 'hills'. EDX measurements further revealed a decrease of the weight percentage of bismuth oxide inside these features. The origin of the observed precipitate is attributed to electrochemical reduction reactions of bismuth ions at the glass surface on the cathode side ($Bi^{3+} + 3e^- \rightarrow Bi^0$). If the reduced Bi associates with the electrode material, it is advantageous energetically: in Bi(n)Me(m) compounds (Me: metal) the chemical potential of Bi decreases, which accelerates the reduction reactions.

4.4. $\chi^{(2)}$ values versus rectification model prediction

The values of $\chi^{(2)}$ increase with increasing $\chi^{(3)}$ of the glass, as predicted by the rectification model but they did not exceed 0.7 pm/V (25.0 mol% Bi_2O_3 glass). Clearly $\chi^{(2)}$ in thermally poled bismuth borate does not really break the limit of thermally poled silica. The relationship between $\chi^{(2)}$ and $\chi^{(3)}$ is sub-linear and has an offset with respect to $\chi^{(2)}$ level in poled silica. Assuming that the rectification model is still valid here ($\chi^{(2)} = 3E_{dc}\chi^{(3)}$) and that the frozen-in field has reached the limit set by dielectric breakdown ($E_{dc} \approx E_b$), this result implies that the dielectric breakdown strength E_b is lower in BZH glasses than in silica and decreases slightly with increasing Bi_2O_3 content. The incorporation of bismuth in the matrix increases the $\chi^{(3)}$ of the glass but, we believe, reduces E_b because electrons in bismuth orbitals are less tightly bonded. If it is the case that high-index glasses have intrinsically low dielectric breakdown strengths (as suggested in [34]), then the enhancement of $\chi^{(2)}$ will not be directly proportional to $\chi^{(3)}$ enhancement and the limit $E_{dc} \leqslant E_b$ must be considered seriously. In practice, a trade-off has to be made between $\chi^{(3)}$ and E_b when one selects glass candidates for enhancing $\chi^{(2)}$ by the rectification model strategy.

5. Summary and conclusion

Second-order optical non-linearity was induced in bismuth borate (Bi_2O_3–ZnO–B_2O_3) and borate (ZnO–B_2O_3) glasses by thermal poling. In the pristine glasses, increasing the Bi_2O_3 content resulted in higher $\chi^{(3)}$ but lower T_g. Poling conditions and current dynamics were

significantly different from those for silica: (1) poling temperatures had to be relatively close to the glass transition temperature (which was much lower than in silica), (2) intimate glass–electrode contact was necessary in order to achieve high and uniform SHG in the poled area, (3) the poling current was much higher than in silica and exhibited very different dynamics depending on Bi_2O_3 content, (4) varying the sample thickness resulted in dramatic changes in the formation dynamics and the amount of $\chi^{(2)}$. In spite of these differences, the non-linearity was located in a near-surface layer at the anode side, like in thermally poled silica. In all cases, the non-linear layer had a thickness lower than SHG coherence length (which decreased with increasing Bi_2O_3 content). The origin of $\chi^{(2)}$ was attributed to the rectification of $\chi^{(3)}$ by the frozen-in field E_{dc} (i.e. $\chi^{(2)} = 3E_{dc}\chi^{(3)}$), but the orientation of dipoles in the form of dangling bonds could not be excluded. It was proposed that the poling mechanism relied on the migration of protons which were released by dissociation of OH bonds and possessed significant mobility at temperatures near T_g. The importance of the glass–electrode contact was explained by the injection of H^+ or H_3O^+ from the atmosphere which tended to neutralize the depletion layer resulting from the migration of internally released H^+. Ionization of the glass was thought to occur and to play a role in the formation dynamics of $\chi^{(2)}$. Electron hopping between multi-valent bismuth ions, on the other hand, did not contribute to the formation of $\chi^{(2)}$ although it did contribute to the poling current. Poling current dynamics were explained qualitatively well by this model. In particular, the dependence of current dynamics on sample thickness was related to the expression of the decay time constant associated with proton migration. The $\chi^{(2)}$ values in thermally poled Bi_2O_3–ZnO–B_2O_3 glasses increased with increasing $\chi^{(3)}$ as predicted by the rectification model, but they did not break the limit of thermally poled silica. From experimentally determined relationship between $\chi^{(2)}$ and $\chi^{(3)}$, it was inferred that the dielectric breakdown strength was lower in Bi_2O_3–ZnO–B_2O_3 glasses than in silica and decreased with increasing Bi_2O_3 content. This result demonstrated the importance to select glass compositions on the basis of *both* $\chi^{(3)}$ and dielectric breakdown strength for the purpose of enhancing $\chi^{(2)}$.

Acknowledgments

O.D. expresses his gratitude to Nippon Sheet Glass Co., Ltd. for financial and technical support of the research project ('High-index Glasses for Poling'). S. Nakagaki is acknowledged for the preparation of the samples. O.D. thanks the Optoelectronics Research Centre at the University of Southampton for his research fellowship (January 2002–December 2003) and the Interuniversity Attraction Pole programme IAP V/18 of the Belgian Science Policy. O.D. dedicates the present article to his father (1933–2003).

References

[1] R.A. Myers, N. Mukherjee, S.R.J. Brueck, Opt. Lett. 16 (1991) 1732.
[2] A. Okada, K. Ishii, K. Mito, K. Sasaki, J. Appl. Phys. 74 (1993) 531.
[3] P.G. Kazansky, A. Kamal, P.St.J. Russell, Opt. Lett. 18 (1993) 693.
[4] T. Fujiwara, D. Wong, Y. Zhao, S. Fleming, S. Poole, M. Sceats, Electron. Lett. 31 (1995) 573.
[5] L.J. Henry, B.V. McGrath, T.G. Alley, J.J. Kester, J. Opt. Soc. Am. B 13 (1996) 827.
[6] P.G. Kazansky, P.St.J. Russell, H. Takebe, J. Lightwave Technol. 15 (1997) 1484.
[7] O. Deparis, C. Corbari, P.G. Kazansky, K. Sakaguchi, Appl. Phys. Lett. 84 (2004) 4857.
[8] P.G. Kazansky, P.St.J. Russell, Opt. Commun. 110 (1994) 611.
[9] H. Nasu, T. Ito, H. Hase, J. Matsuoka, K. Kamiya, J. Non-Cryst. Solids 204 (1996) 78.
[10] K. Tanaka, A. Narazaki, K. Hirao, Opt. Lett. 25 (2000) 251.
[11] B.V.R. Chowdari, Z. Rong, Solid State Ionics 90 (1996) 151.
[12] R.W. Boyd, Nonlinear optics, Academic, 1992.
[13] P. Becker, Cryst. Res. Technol. 38 (2003) 74.
[14] J. Jerphagnon, S.K. Kurtz, J. Appl. Phys. 41 (1970) 1667.
[15] P.D. Maker, R.W. Terhune, M. Nisenoff, C.M. Savage, Phys. Rev. Lett. 8 (1962) 21.
[16] D. Faccio, V. Pruneri, P.G. Kazansky, Appl. Phys. Lett. 79 (2001) 2687.
[17] C. Corbari, O. Deparis, B.G. Klappauf, P.G. Kazansky, Electron. Lett. 39 (2003) 197.
[18] M. Qiu, T. Mizunami, R. Vilaseca, F. Pi, G. Orriols, J. Opt. Soc. Am. B 19 (2002) 37.
[19] N.P. Bansal, R.H. Doremus, Handbook of glass properties, Academic, New York, 1986.
[20] G. Wallis, D.I. Pomerantz, J. Appl. Phys. 40 (1969) 3946.
[21] N. Mukherjee, R.A. Myers, S.R.J. Brueck, J. Opt. Soc. Am. B 11 (1994) 665.
[22] T.G. Alley, S.R.J. Brueck, M. Wiednbeck, J. Appl. Phys. 86 (1999) 6634.
[23] T.G. Alley, S.R.J. Brueck, R.A. Myers, J. Non-Cryst. Solids 242 (1998) 165.
[24] C.J.S. Matos, I.C.S. Carvalho, E.F. da Silveira, W. Margulis, R.R. Pinho, B. Lesche, J. Non-Cryst. Solids 273 (2000) 25.
[25] B. Kusz, K. Trzebiatowski, R.J. Barczynski, Solid State Ionics 159 (2003) 293.
[26] S.P. Yawale, S.V. Pakade, J. Mater. Sci. 28 (1993) 5451.
[27] H. Behrens, R. Kappes, P. Heitjans, J. Non-Cryst. Solids 306 (2002) 271.
[28] A. von Hippel, E.P. Gross, J.G. Jelatis, M. Geller, Phys. Rev. 91 (1953) 568.
[29] T.M. Proctor, P.M. Sutton, J. Am. Ceram. Soc. 43 (1960) 173.
[30] D.E. Carlson, J. Am. Ceram. Soc. 57 (1974) 291.
[31] D.E. Carlson, K.W. Hang, G.F. Stockdale, J. Am. Ceram. Soc. 57 (1974) 295.
[32] R.J. Barczynski, L. Murawski, J. Non-Cryst. Solids 307 (2002) 1055.
[33] F.C. Garcia, I.C.S. Carvalho, E. Hering, W. Margulis, Appl. Phys. Lett. 72 (1998) 3252.
[34] A.L.R. Brennand, P.G. Kazansky, J.S. Wilkinson, Techn. Digest of CLEO, 2002, p. 236.